Performance Investigation on Cascade Latent Heat Storage for Various Geometric Orientations

Shubham Jain[1], K. Ravi Kumar[1], Dibakar Rakshit[1], B. Premachandran[2], K. S. Reddy[3]

[1]Department of Energy Science and Engineering, Indian Institute of Technology Delhi, (India)

[2]Department of Mechanical Engineering, Indian Institute of Technology Delhi, (India)

[3]Department of Mechanical Engineering, Indian Institute of Technology Madras, (India)

Abstract

Storing solar thermal energy in the form of the latent heat of the phase change materials (PCMs) is a widely adopted method to assist energy applications in a sustainable manner. The cascading of the PCMs in a latent heat storage unit improves the uniformity of the heat transfer process. In this investigation, all the configurations of the storage (two single PCM-based storage having $NaNO_3$ and $NaNO_2$ as the PCMs and the 2-stage multi-PCM storage having both the PCMs) are designed to store the 1 MJ of latent thermal energy. The present study highlights that a 35.23% and 10.52% enhanced charging rate can be achieved in the 2-stage cascade latent heat storage (CLHS) than the single PCM-based storages, i.e., $NaNO_3$ and $NaNO_2$. Furthermore, the present study is extended to underline the effect of the geometric orientation of the CLHS over the melting behavior of the CLHS. The melt cycle time of the horizontal CLHS was found to be 39.04%, 15.78%, and 5.9% less than the corresponding charging time of the 1-stage $NaNO_3$ storage, 1-stage $NaNO_2$ storage, and 2-stage vertical CLHS, respectively. Although the horizontal orientation of the storage can enhance the melting rate in the PCMs of the CLHS, it is more suited for the part load charging conditions.

Keywords: Solar Thermal Energy Systems, Latent Heat Storage, Phase Change Materials, Computational Fluid Dynamics, Cascade Thermal Energy Storage.

1. Introduction

For sustainable development, a reduction in the dependency on fossil fuels is necessary. The inclination of the present generation toward renewable energy is the way to opt for eco-friendly solutions for the current energy demands. Solar energy is one of the widely opted energy resources to replace conventional energy resources. The unavailability of the Sun during the night and variable solar radiation intensity are the major shortcomings of the utilization of solar energy for various energy applications. Dedicated thermal energy storage can solve these problems. There are three ways to store the thermal energy of the Sun, i.e., in the form of the increased temperature of the medium (sensible thermal energy storage (STES)), in the form of phase transition enthalpy (latent thermal energy storage (LTES)) and in the form of the enthalpy of the chemical reactions (thermochemical energy storage (TCES)). In terms of maturity, STES is the most widely used storage solution for solar thermal applications. The problem of the low energy density of the STES can be solved using TCES, but the cost and the complications involved in the storage process restricts their commercial implementations. In terms of the high energy density, easy availability, easy operational cycle, and low cost, LTES (stores energy in the phase change materials (PCMs)) is one of the preferred storage solutions in solar thermal applications. The low thermal conductivity of the PCMs and non-uniform melting/solidification of the large volume LTES are the shortcomings on which researchers are working (Ray et al., 2021). The incorporation of conductive materials and structures such as metallic nanoparticles, metallic porous structures in the PCMs, and the use of extended surfaces are methods to solve the problem of low thermal conductivity of the PCMs, while the cascading of the PCMs in the single LTES can improve the process uniformity during the storing/retrieving cycle of the storage (Jain et al., 2021). Tiary et al. (Tiari et al., 2021) have investigated the effect of using the annular fins and reported a significant improvement in the charging process on increasing the fin length. The 30.3% and 28.2% reduction in the charge and discharge time, respectively, were reported by Wu et al. in the nano-enhanced paraffin (Wu et al., 2010). Efforts are made to enhance the performance of the LTES using heat pipes also. Another feasible technique of heat transfer augmentation is the utilization of porous metallic structures in the storage medium. Sardari et al. (Sardari et al.,

doi:10.18086/eurosun.2022.13.12 Available at http://proceedings.ises.org

2019) have reported an 85% reduction in the charge cycle time of the storage by using porous copper foam.

The cascading of the storage materials (PCMs) in the LTES unit can improve the process uniformity in the heat transfer between HTF and PCM, which results in the enhanced charging/discharging rate of the storage. Adine et al. (Adine and El Qarnia, 2009) have evaluated the performance of a 2-stage CLHS having organic PCMs. In this study, 2-stage CLHS was found to be more effective. Piero et al. (Peiró et al., 2015) have reported a 19.36% improvement in the effectiveness of the CLHS than the 1-stage. Researchers have analysed the CLHS with the hybrid enhancement of heat transfer also. In such a study, Shabgard et al. (Shabgard et al., 2012) highlighted the improved performance of the CLHS using heat pipes.

A few studies can be found that highlight the effect of the orientation on the performance of the single PCM storage. The effect of the orientation on the charging performance of the CLHS has not been investigated thoroughly. Here in the present study, efforts are made to underline the effect of the no. of stages on the charge cycle behavior of the CLHS as well as the effect of the geometric orientation of the CLHS on the energy storage process of the CLHS. The change in the energy transfer rate of the storage medium in one stage may affect the melting rate of the PCM in another stage. The present work will highlight the charging behavior of the CLHS for various geometric orientations, such as vertical and horizontal.

2. Numerical Modelling and Governing Equations

2.1. Description of the Model

In the present work, shell and tube-type LTES units having single and multiple PCMs on the shell sides are investigated. The study is further extended to highlight the charging performance of the storage for two different orientations, i.e., vertical and horizontal. The hot HTF flows through the concentric inner tube to transfer the thermal energy to the PCMs (Figure: 1). The storage configurations are designed to store 1 MJ of latent thermal energy (calculated based on average energy density). The storage consists of stainless steel (SS316) shell (outer diameter of 73 mm and thickness of 2.11 mm) and an inner concentric tube made of copper (outer diameter of 22.22 mm and thickness of 1.65 mm). The PCMs are kept shell side while the HTF flows through the inner copper tube. The total length of the storage is chosen as 888 mm, and the shell compartments are divided into equal lengths for storing multiple PCMs, as shown in Figure: 1. Here, attempts are made to develop a low-cost shell and tube-based CLHS to support the energy demand of the medium temperature applications. Therefore, $NaNO_3$ and $NaNO_2$ having melting temperatures of 579 K and 555 K, respectively, are utilized as the PCMs. Thermal oils are one of the widely used heat transfer fluids (HTF) for low to medium-temperature applications. Therefore, Therminol 66 is utilized here as the working HTF. The properties of the PCMs and HTF used in the study are given in Table: 1. Initially, the thermal performance of the two single PCM-based storage having $NaNO_3$ and $NaNO_2$ as the PCMs is compared with the thermal performance of the 2-stage CLHS having both the PCMs in the single unit for the charging cycle. Moreover, the performance of the cascade storage is further evaluated for the two different orientations such as vertical and horizontal.

2.2. Assumptions

The following assumptions are incorporated into the present model:

- All the phases of utilized materials are considered homogeneous and isotropic.
- The melted PCM is assumed to behave as a Newtonian fluid.
- The radiation heat transfer, volume variation during phase change, and viscous energy dissipation are neglected here.
- The Boussinesq assumption is used to model the natural convection in the PCMs.
- The insulated boundary condition is provided on the outer exposed wall of each configuration of the storage.

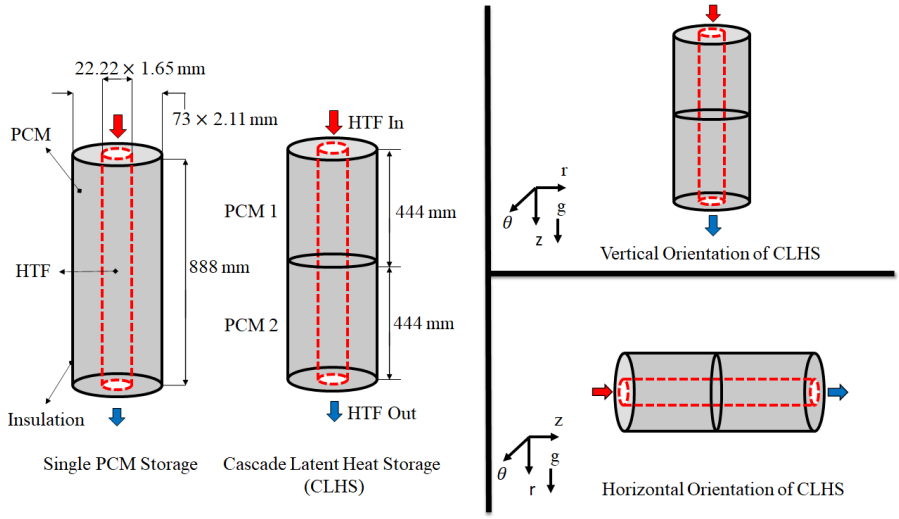

Fig. 1: Schematic of the storage configurations investigated in the present study

Tab. 1: Thermo-physical properties of PCMs and HTF used in the study (Alekseeva et al., 2019; Janz et al., 1979; Marušić and Lončar, 2020; Tiari et al., 2015)

Properties	**$NaNO_3$**	**$NaNO_2$**	**HTF**
Melting Temperature (K)	579	555	-
Phase Transition Enthalpy (kJ/kg)	176	180.12	-
Expansion Coefficient (1/K)	0.0004	0.00028	-
Specific Heat Capacity (kJ/kg K)	1.60 (s), 1.655 (l)	1.733 (s), 2.553 (l)	2.73
Thermal Conductivity (W/m-K)	0.8 (s), 0.68 (l)	0.765 (s), 0.665 (l)	0.0893
Density (kg/m^3)	1908	1812	775
Dynamic Viscosity $\times 10^{-4}$ (Pa-s)	26.9	26.66	3.36

2.3. Governing Equations

The phase transition process of the storage is modeled here using the 'Enthalpy Porosity Method' (Brent et al., 1988). The governing equations involved in the method are given below:

HTF:

Mass conservation equation:

$$\frac{\partial \rho_f}{\partial t} + \nabla \cdot \left(\rho_f \vec{V}\right) = 0 \qquad \text{(eq. 1)}$$

Momentum conservation equation:

$$\rho_f \left(\frac{D\vec{V}}{Dt}\right) = -\nabla \mathrm{p} - \frac{2}{3}\nabla\left(\mu_f \nabla \cdot \vec{V}\right) + \nabla \cdot \left[\mu_f\left(\nabla\vec{V} + \left(\nabla\vec{V}\right)^T\right)\right] \qquad \text{(eq. 2)}$$

Energy conservation equation:

$$\rho_f c_{p_f} \left(\frac{DT}{Dt}\right) = \nabla \cdot (\mathrm{k}_f \nabla \mathrm{T}) \qquad \text{(eq. 3)}$$

PCM:

Mass conservation equation:

$$\frac{\partial \rho}{\partial t} + \nabla \cdot \left(\rho \vec{V}\right) = 0 \quad \text{(eq. 4)}$$

Momentum conservation equation:

$$\frac{\partial \rho \vec{V}}{\partial t} + \nabla \cdot \left(\rho \vec{V} \vec{V}\right) = -\nabla p + \vec{g} \beta_t \rho_{ref} \left(T - T_{ref}\right) + \nabla \cdot \left(\mu \nabla \vec{V}\right) + \vec{S}_M \quad \text{(eq. 5)}$$

Here,

$$\vec{S}_M = -\frac{(1-\beta)^2}{\beta^3 + \varepsilon} A_{Mushy} \vec{V} \quad \text{(eq. 6)}$$

Here, A_{Mushy} is taken as 10^5 (Fadl and Eames, 2019). The body force term is included as $g \beta_t \rho_{ref} \left(T - T_{ref}\right)$ using Boussinesq approximation.

Energy conservation equation:

$$\frac{\partial (\rho H_t)}{\partial t} + \nabla \cdot \left(\rho \vec{V} H_t\right) = \nabla \cdot (k \nabla T) \quad \text{(eq. 7)}$$

The total enthalpy is further expressed as:

$$H_t = h_s + h_l \quad \text{(eq. 8)}$$

Here,

$$h_s = h_{ref} + \int_T^{T_m} C_p \partial T \quad \text{(eq. 9)}$$

$$h_l = \beta L \quad \text{(eq. 10)}$$

Melt fraction (β):

$$\beta = \begin{cases} \frac{T - T_{Solidus}}{T_{Liquidus} - T_{Solidus}}; & \text{when } T_{Solidus} < T < T_{Liquidus} \\ 0; & \text{when } T \leq T_{Solidus} \\ 1; & \text{when } T \geq T_{Liquidus} \end{cases} \quad \text{(eq. 11)}$$

2.4. Initial and Boundary Conditions

The initial domain temperature and the inlet HTF temperature are taken as 519K and 615 K, respectively. The HTF velocity considered in the analysis is 0.04 m/s. Furthermore, the following boundary and initial conditions are used in the modeling of the process:

HTF:

At $t = 0: \vec{v} = 0, T = T_{initial}$ (eq. 12)

At $r = r_i: \vec{v} = 0, T_{itf^+} = T_{itf^-}$ (eq. 13)

At $z = 0: u = u_{in},\ T = T_{in}$ (eq. 14)

At $z = l_{st}: p = p_0$ (eq. 15)

PCM:

At $t = 0: \vec{v} = 0, T = T_{initial}$ (eq. 16)

At $r = r_o: \vec{v} = 0,\ T_{itf^+} = T_{itf^-}$ (eq. 17)

At $r = R_i: \vec{v} = 0,\ \frac{\partial T}{\partial r} = 0$ (eq. 18)

At $z = 0: \vec{v} = 0,\ \frac{\partial T}{\partial z} = 0$ (eq. 19)

At $z = l_{st}$: $\vec{v} = 0,\ \frac{\partial T}{\partial z} = 0$ (eq. 20)

At $z = \frac{l_{st}}{2}$: $\vec{v} = 0,\ \frac{\partial T}{\partial z} = 0$ (for two-stage cascade storage) (eq. 21)

2.5. Validation of Numerical Model and Solution Procedure

The grid independence study and the time step independence study have highlighted that the 697500 elements and the time step size of 0.1s are appropriate for the numerical model (Figure: 2). The developed model is validated by using the results of the experimental study performed by Hosseini et al. (Hosseini et al., 2012). (Figure: 3). A maximum deviation of 2.5 K and 4.1 K in average and local temperature of the PCM is reported here (Hosseini et al., 2012).

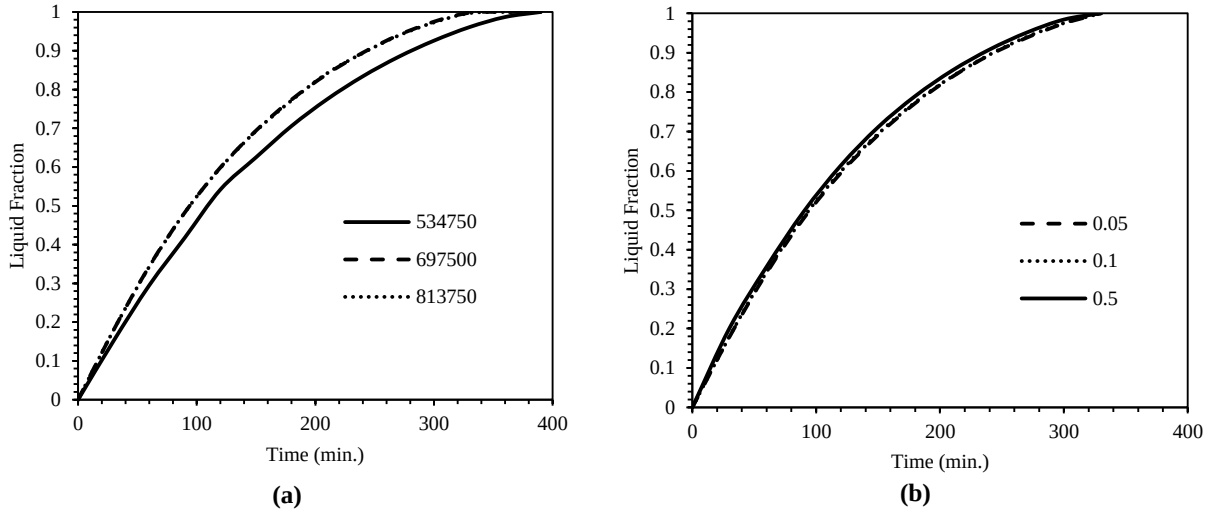

Fig. 2: (a) Grid independence study (b) Time step independence study

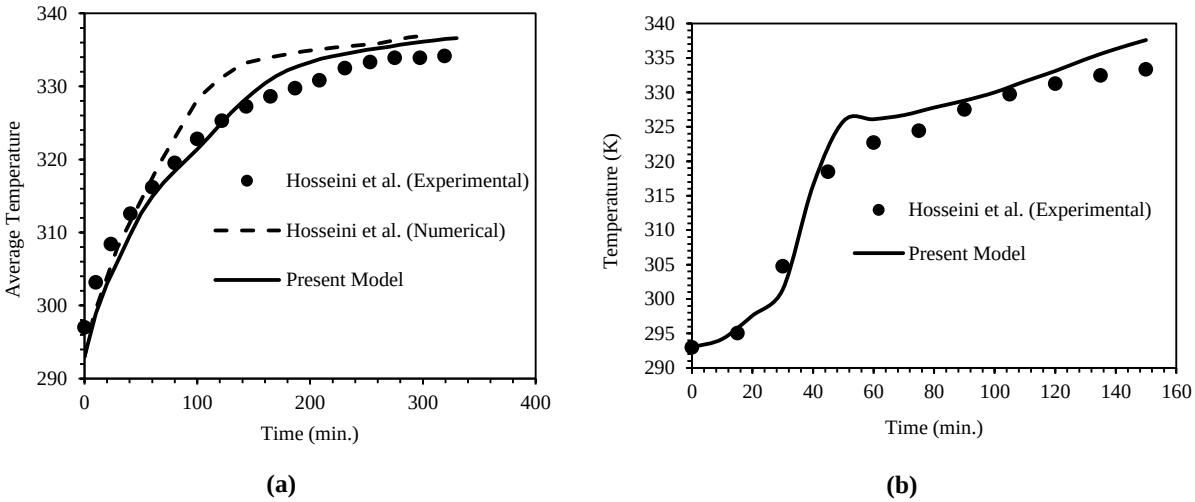

Fig. 3: Model validation (Hosseini et al., 2012) (a) Average temperature of the phase change material, (b) Local temperature in the phase change material

3D models are prepared for each configuration of the storage , and unsteady state simulations are performed using ANSYS Fluent 2020 R1 (ANSYS Inc (Release-15.0), 2015), where a pressure-based solver and SIMPLE algorithm are implemented (Mekrisuh et al., 2020). Here QUICK scheme is used for discretization, and pressure staggering option (PRESTO) is also incorporated (Mekrisuh et al., 2020). A convergence criterion of 10^{-3} is assigned for both mass and momentum equations, and on the other hand, a convergence criterion of 10^{-6} is assigned for the energy equation in the present numerical model.

3. Results and Discussion

In the present study, a comparative charge cycle performance evaluation is done between two single PCM-based vertical LTES having $NaNO_3$ and $NaNO_2$ as the PCMs and the two-stage vertical CLHS having both the PCMs together in a single storage unit. Moreover, the current study is extended further to highlight the effect of the geometric orientation (vertical and horizontal) of the storage on the melting cycle of the storage. All the storage configurations are designed to store the 1 MJ of latent thermal energy. The findings of the current study are as follows:

3.1. Comparative Assessment of Single and Multiple PCM-based Storage

Initially, a comparative analysis is done to highlight the effect of the cascading of the PCMs in a vertical LTES unit. In this context, the melting process in single-stage $NaNO_3$, $NaNO_2$, and two-stage $NaNO_3$/ $NaNO_2$ vertical storages is investigated. The HTF enters from the top of the storage and transfers heat to the surrounding PCM shell. The melting process is initiated almost at the same time (after 30 minutes) in $NaNO_3$ and $NaNO_3$/ $NaNO_2$ storage, while $NaNO_2$ shows an early initiation (after 20 minutes) of the melting process (Figure: 4 (a)). Owing to the significant temperature differential between the HTF and the phase transition temperature of the $NaNO_2$, a fast-charging rate can be seen at the initial stage of the melting. As the HTF passes through the inner HTF tube in the storage, the temperature of the HTF decreases, which further reduces the established energy transfer rate from HTF to the storage medium (PCM). The arrangement of the two different PCMs in the HTF movement direction having PCM of higher phase transition temperature in the primary stage maintains a better rate of heat transfer between HTF and PCM, which improves the charging process. Here $NaNO_3$, $NaNO_2$, and $NaNO_3$/ $NaNO_2$ configurations of the storage complete the melting after 525 minutes, 380 minutes, and 340 minutes, respectively of the charging process. The time of the complete charging of the 2-stage CLHS is found to be 35.23% and 10.52% less as compared to the $NaNO_3$ and $NaNO_2$ storage. Both the stages of the CLHS complete the melting after a nearly equal time period (stage 1 in 340 minutes, while stage 2 in 330 minutes), which is the best way to utilize the CLHS technology. Figure: 4(b) represents the variation of the average temperature of the PCMs in each configuration of the storage. The three different stages (sensible heating of solid PCM, phase transition, and the sensible heating of the liquid PCM) of the charging cycle of the LTES can be seen in the figure. $NaNO_3$ has a higher melting temperature as compared to $NaNO_2$; therefore, a long sensible heating phase can be seen in figure: 4(b). After the initiation of the melting, a slight increment in PCM temperature can be seen until the completion of the charging cycle. After that, it achieves a temperature equal to the inlet temperature of the HTF to complete the charging cycle. All the other PCMs follow the same trend to complete the charging cycle.

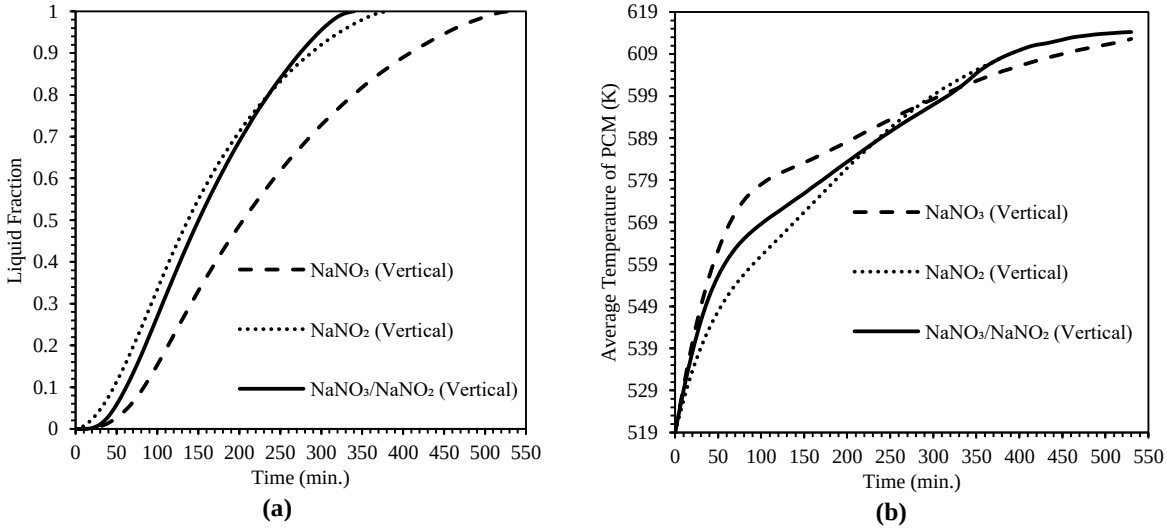

Fig. 4: (a) Variation of the liquid faction of the PCMs in the vertical storage configurations (b) Variation of the average temperature of the PCMs in the vertical storage configurations

A clear depiction of the melting front movement can be seen in Figures: 5 and 6. Figure: 5 represents the movement of the melt front on the central axial plane in the storage, while Figure: 6 represents the movement of the melt front on the two radial planes at an axial location of 222 mm (top) and 666 mm (bottom) from the inlet. In the vertical storage configurations, the HTF enters from the top of the storage and transfers energy to the PCM

through the adjacent copper wall; as the PCM starts melting, buoyancy-driven natural convection sets up in the PCM domain. Due to the low density of the liquid PCM, it tries to pile up at the top portion of the storage. The accumulation of the PCM at the top portion of the vertical storage enhances the energy transfer in that region. Therefore, a faster rate of energy transfer can be depicted in figure: 6 as compared to the bottom portion of the storage.

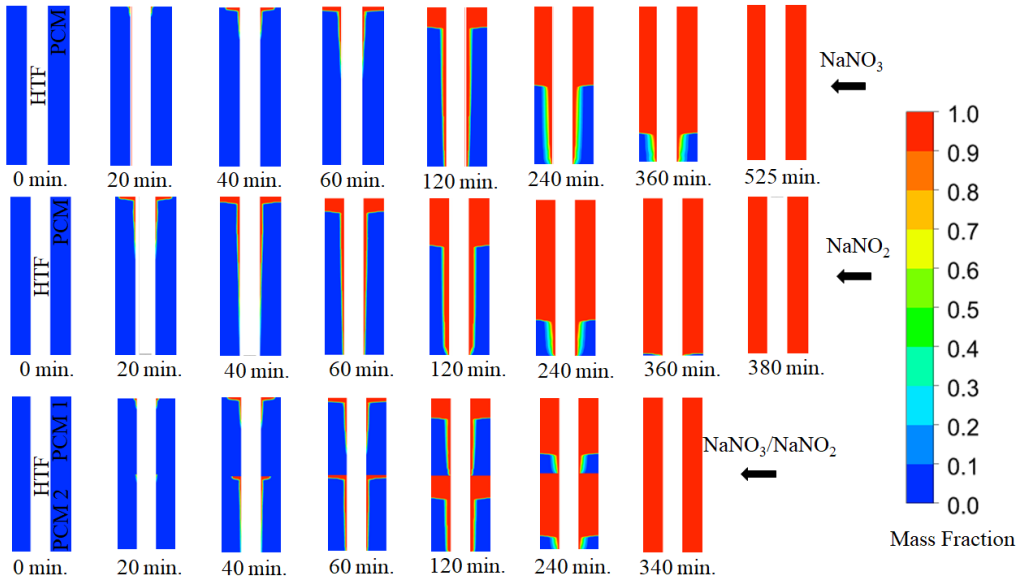

Fig. 5: Liquid faction contours in the vertical storage configurations (at a central axial plane)

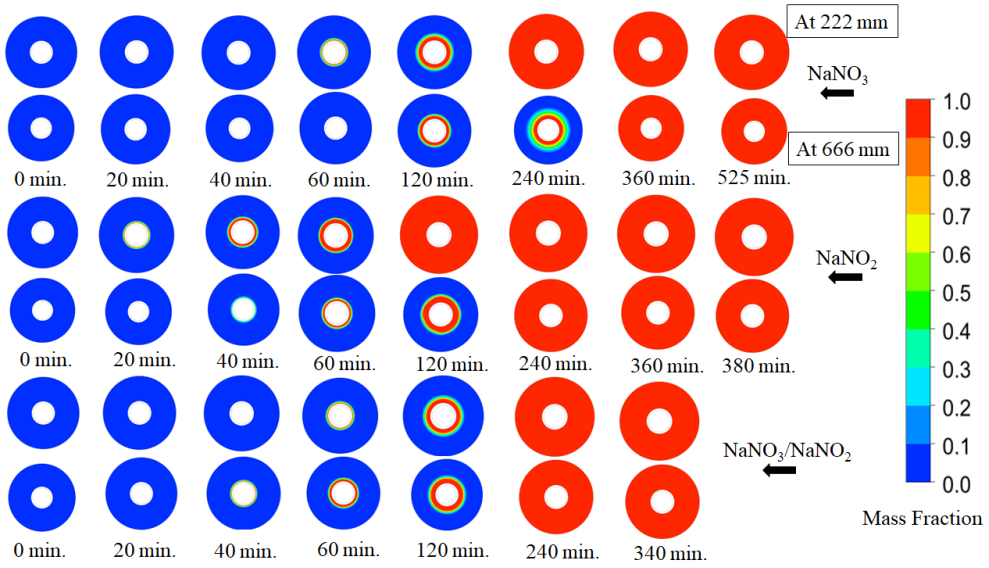

Fig. 6: Liquid faction contours in the vertical storage configurations (at the radial plane located at an axial distance of 222 mm (top) and 666 mm (bottom) from the inlet)

Figure: 7 represents the temperature contours on the axial plane in storage . It can be inferred from the figure that stage 2 has lower temperature distribution as compared to stage 1 of the CLHS because it reaches the melting state earlier than stage 1, as explained above. The significant movement of the melted PCM at the top region of the storage augments the rate of melting, which results in the high temperature of the PCM in that region.

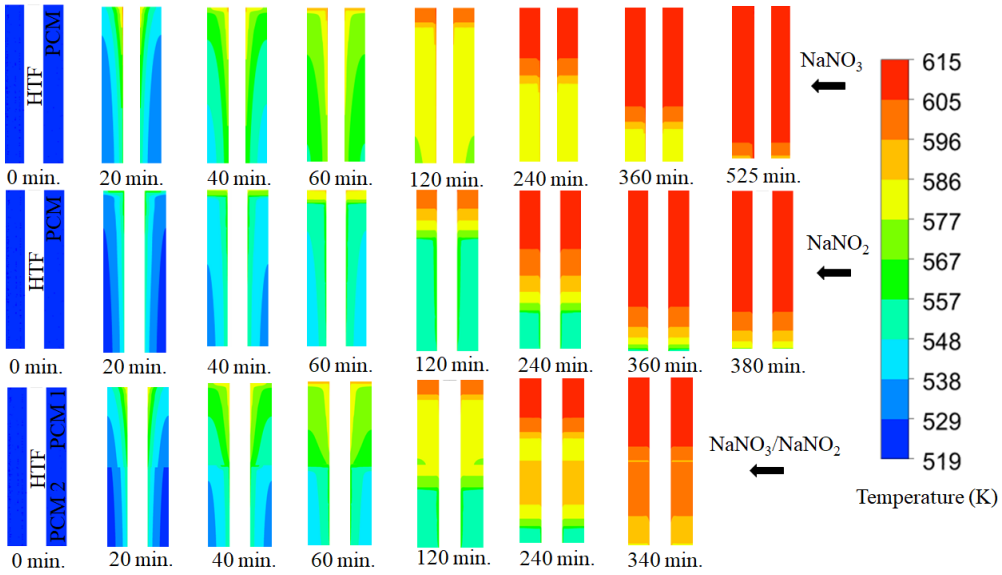

Fig. 7: Temperature contours in the vertical storage configurations (at a central axial plane)

3.2. Comparative Assessment of Cascade Latent Heat Storage for Various Geometric Orientations

The present study is further extended to investigate the effects of the various orientations of the CLHS on the charging process. In this context, the 2-stage CLHS is investigated for the vertical and horizontal orientations. The variation of the average melt fraction in the CLHS and the variation of the average melt fraction in the individual stage of the CLHS can be seen in Figure: 8. During the sensible heating of the solid PCMs, the conduction heat transfer will be dominant, due to which both the storages behave the same.

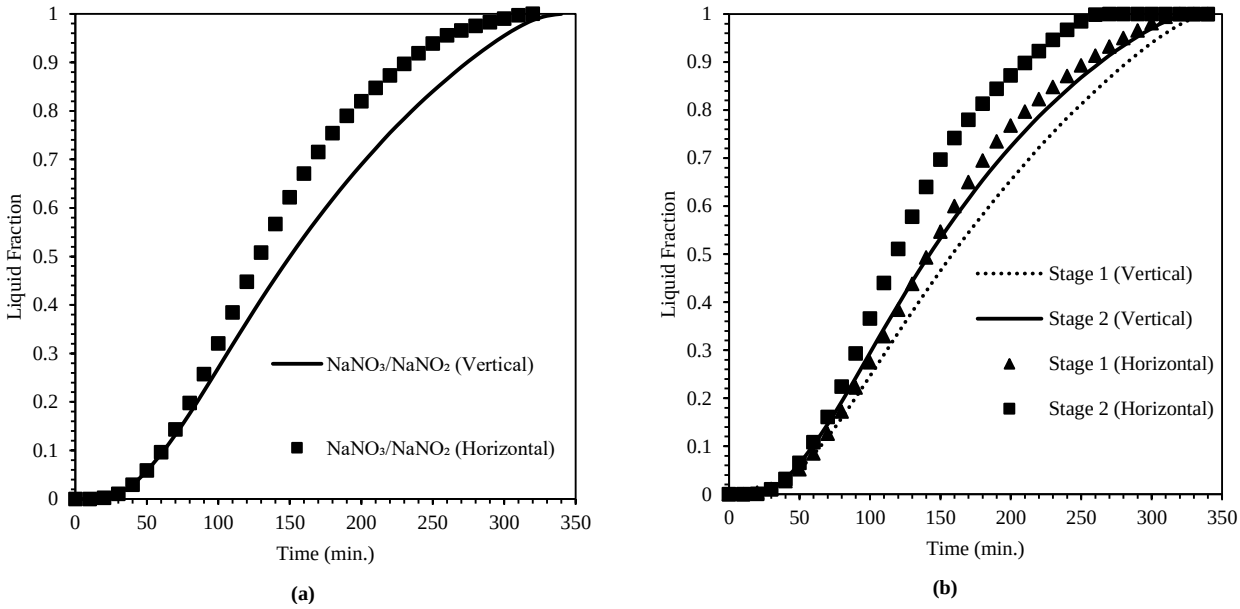

Fig. 8: Variation of the liquid faction of the PCMs in the vertical and horizontal CLHS (a) Average liquid fraction in CLHS (b) average liquid fraction in individual stages of CLHS

It can be depicted from the figure that initially, both vertical and horizontal CLHS shows the same rate of melting because of weak natural convection due to the less mass of the melted PCMs in each stage. After 70 minutes of the charging operation, a difference in the rate of melting can be seen in both configurations. As explained in the earlier section that due to the low density of the melted PCM, a natural convection current sets up in the domain which tries to move the liquid PCM in the opposite direction of the gravity (buoyancy-driven motion).

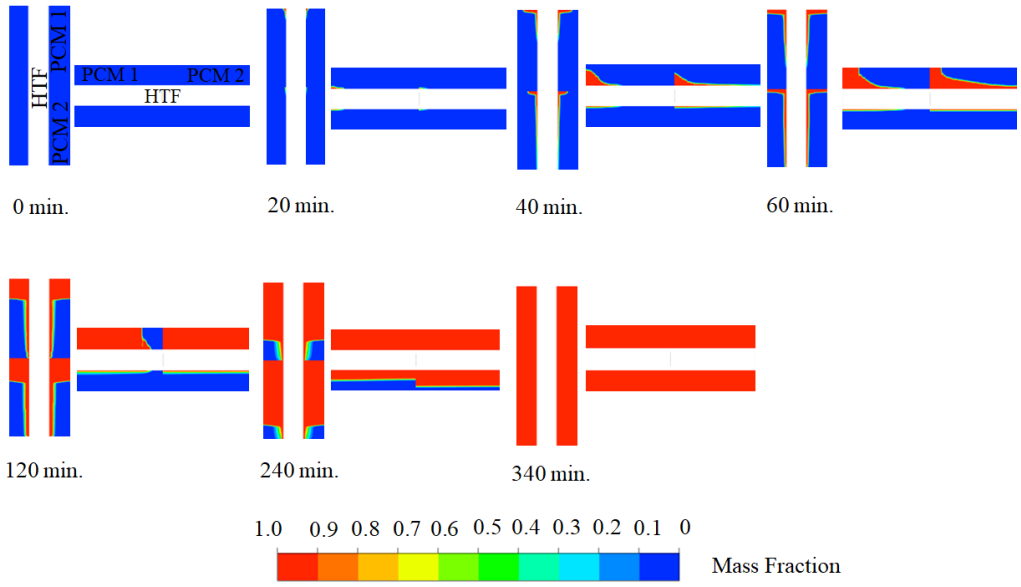

Fig. 9: Liquid faction contours in the vertical (left) and horizontal (right) CLHS (at a central axial plane)

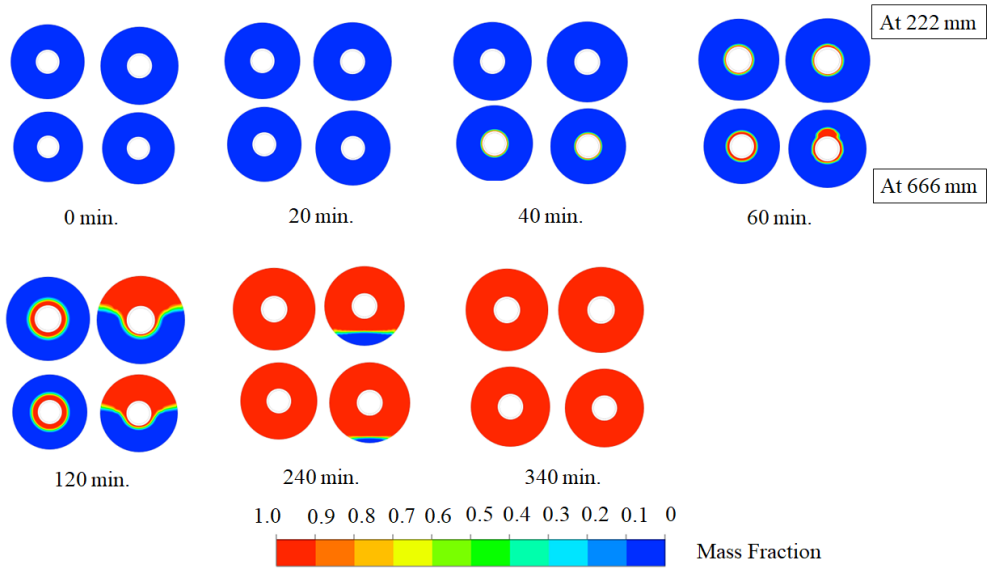

Fig. 10: Liquid faction contours in the vertical (left) and horizontal (right) CLHS (at the radial plane located at an axial distance of 222 mm (top) and 666 mm (bottom) from the inlet)

The gravitational force acts toward the HTF flow direction (z-direction) in the vertical orientation, while it acts in the radial direction (r direction) in the horizontal orientation. So, in the vertical orientation, the melted PCM tries to pile up in the top portion of the storage and improve the rate of heat transfer in that portion, which ultimately slows down the phase transition in the bottom portion of the storage (Figure: 9, 10). Conversely, in the horizontal orientation, the PCM tries to move in the radial direction (perpendicular to the HTF flow direction) and improves the heat transfer along the entire length of the storage (Figure: 9, 10). Therefore, a better charging rate can be seen in the horizontal CLHS as compared to the vertical CLHS.

An important observation can be made from the Figure: 9, and 10, that in horizontal CLHS, after the completion of the melting in the upper half domain of the CLHS, the rate of the heat transfer remains slow during the melting of the lower half domain of the CLHS due to accumulation of the melted PCM opposite to the direction of the gravity. Therefore, a slow rate of melting can be seen after the 50% charging of the storage. Therefore, it can be inferred that horizontal orientation is more suited for the part load operation of the CLHS. The charging period of the horizontal CLHS was found to be 39.04%, 15.78%, and 5.9% less than the charging period of the 1-stage $NaNO_3$ storage, 1-stage $NaNO_2$ storage, and 2-stage vertical CLHS, respectively (Figure: 11 (a)). In vertical CLHS, stage 2 (after 320 minutes of the charging operation) completes the melting 20 minutes earlier than stage

1(after 340 minutes of the charging operation) because of the high-temperature difference between the HTF (heat carrier fluid) and the melting temperature of the PCM in stage 2. However, in the horizontal CLHS, stage 2 (after 270 minutes of the charging operation) completes the melting 50 minutes earlier than stage 1(after 320 minutes of the charging operation). Therefore, it can be inferred that the orientation of the LTES affects the comparative melting behavior of the individual stage and increase the time range of the operation of the CLHS (Figure: 8(b)). Another essential parameter to judge the performance of the LTES is the total latent thermal energy stored during the complete charging process. Figure: 11 (b) represents the latent heat stored in the various configurations of the storage. All the configurations of the storage are designed to store 1 MJ of latent heat. It is inferred from the figure that after the 320 minutes of the charging process, 1-stage $NaNO_3$, 1-stage $NaNO_2$, and 2-stage vertical CLHS store 78%, 93%, and 98%, respectively, of the target latent thermal energy, while horizontal 2-stage CLHS is the only storage configuration which stores the 100% of the targeted energy.

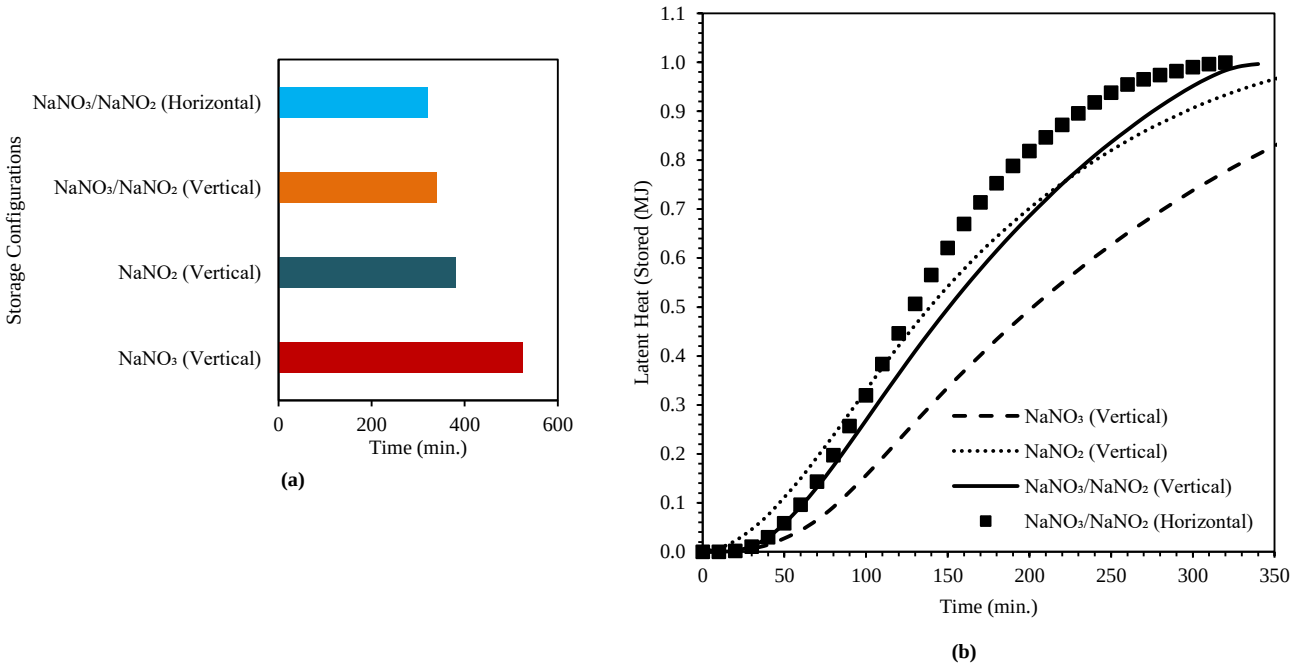

Fig. 11: (a) Total melting time of the storage configurations investigated in the present study (b) Latent thermal energy stored in the storage configurations investigated in the present study

4. Conclusion

In this investigation, a comparative thermal performance evaluation of the single PCM-based latent heat storage having $NaNO_3$ and $NaNO_2$ as the PCMs and the 2-stage cascade latent heat storage having both the PCMs is done. It is concluded that a 35.23% and 10.52% faster-charging rate than single PCM-based counterparts, i.e., $NaNO_3$ storage and $NaNO_2$ storage, respectively, can be obtained using 2-stage CLHS. The movement and accumulation of the liquid PCM at the top portion of the vertical storage slow down the melting in the other lower part of the storage. The use of any heat transfer enhancement method for the lower portion of the storage can boost the melting rate of the entire storage. Moreover, the present study also concludes that the charge cycle performance of the vertical CLHS can be reduced further by changing the orientation of the CLHS to horizontal. The charge cycle time of the horizontal CLHS was found to be 39.04%, 15.78%, and 5.9% less than the charge cycle time of the 1-stage $NaNO_3$ storage, 1-stage $NaNO_2$ storage, and 2-stage vertical CLHS, respectively. It also concluded that after the 320 minutes of the charging process, 1-stage $NaNO_3$, 1-stage $NaNO_2$, and 2-stage vertical CLHS store 78%, 93%, and 98%, respectively, of the target latent thermal energy, while horizontal 2-stage CLHS is the only storage configuration which stores the 100% of the targeted energy. The present study can further be extended for the discharging cycle to highlight the cyclic behavior of the multiple PCM-based storage.

Acknowledgments

The financial support for this research work is provided by the Department of Science and Technology (DST), Government of India, New Delhi, through the research project (Project Number: DST/TMD/CERI/RES/2020/14(G)).

References

Adine, H.A., El Qarnia, H., 2009. Numerical analysis of the thermal behaviour of a shell-and-tube heat storage unit using phase change materials. Appl. Math. Model. 33, 2132–2144. https://doi.org/10.1016/j.apm.2008.05.016

Alekseeva, O.A., Naberezhnov, A.A., Chernyshov, D.Y., Fokin, A.V., Sysoeva, A.A., Rysiakiewicz-Pasek, E., 2019. Thermal expansion coefficients of NaNO2 embedded into the nanoporous glasses. Nanosyst. Physics, Chem. Math. 10, 158–163. https://doi.org/10.17586/2220-8054-2019-10-2-158-163

ANSYS Inc (Release-15.0), 2015. ANSYS Fluent Theory Guide. ANSYS Inc., USA 15317, 1–759.

Brent, A.D., Voller, V.R., Reid, K.J., 1988. Enthalpy-porosity technique for modeling convection-diffusion phase change: Application to the melting of a pure metal. Numer. Heat Transf. 13, 297–318. https://doi.org/10.1080/10407788808913615

Fadl, M., Eames, P.C., 2019. Numerical investigation of the influence of mushy zone parameter Amush on heat transfer characteristics in vertically and horizontally oriented thermal energy storage systems. Appl. Therm. Eng. 151, 90–99. https://doi.org/10.1016/j.applthermaleng.2019.01.102

Hosseini, M.J., Ranjbar, A.A., Sedighi, K., Rahimi, M., 2012. A combined experimental and computational study on the melting behavior of a medium temperature phase change storage material inside shell and tube heat exchanger. Int. Commun. Heat Mass Transf. 39, 1416–1424. https://doi.org/10.1016/j.icheatmasstransfer.2012.07.028

Jain, S., Kumar, K.R., Rakshit, D., 2021. Heat transfer augmentation in single and multiple (cascade) phase change materials based thermal energy storage: Research progress, challenges, and recommendations. Sustain. Energy Technol. Assessments 48, 101633. https://doi.org/10.1016/j.seta.2021.101633

Janz, G.J., Allen, C.B., Bansal, N.P., Murphy, R.M., Tomkins, R.P.T., 1979. Physical Properties Data Compilations Relevant To Energy Storage - 2. Molten Salts: Data on Single and Multi-Component Salt Systems., National Bureau of Standards, National Standard Reference Data Series.

Marušić, A., Lončar, D., 2020. Experimental validation of high-temperature latent heat storage model using melting front propagation data. Appl. Therm. Eng. 164. https://doi.org/10.1016/j.applthermaleng.2019.114520

Mekrisuh, K. u., Singh, D., Udayraj, 2020. Performance analysis of a vertically oriented concentric-tube PCM based thermal energy storage system: Parametric study and correlation development. Renew. Energy 149, 902–916. https://doi.org/10.1016/j.renene.2019.10.074

Peiró, G., Gasia, J., Miró, L., Cabeza, L.F., 2015. Experimental evaluation at pilot plant scale of multiple PCMs (cascaded) vs. single PCM configuration for thermal energy storage. Renew. Energy 83, 729–736. https://doi.org/10.1016/j.renene.2015.05.029

Ray, A.K., Rakshit, D., Ravi Kumar, K., Gurgenci, H., 2021. Silicon as high-temperature phase change medium for latent heat storage: A thermo-hydraulic study. Sustain. Energy Technol. Assessments 46, 101249. https://doi.org/10.1016/j.seta.2021.101249

Sardari, P.T., Mohammed, H.I., Giddings, D., walker, G.S., Gillott, M., Grant, D., 2019. Numerical study of a multiple-segment metal foam-PCM latent heat storage unit: Effect of porosity, pore density and location of heat source. Energy 189, 116108. https://doi.org/10.1016/j.energy.2019.116108

Shabgard, H., Robak, C.W., Bergman, T.L., Faghri, A., 2012. Heat transfer and exergy analysis of cascaded latent heat storage with gravity-assisted heat pipes for concentrating solar power applications. Sol. Energy 86, 816–830. https://doi.org/10.1016/j.solener.2011.12.008

Tiari, S., Hockins, A., Mahdavi, M., 2021. Numerical study of a latent heat thermal energy storage system

enhanced by varying fin configurations. Case Stud. Therm. Eng. 25, 100999. https://doi.org/10.1016/j.csite.2021.100999

Tiari, S., Qiu, S., Mahdavi, M., 2015. Numerical study of finned heat pipe-assisted thermal energy storage system with high temperature phase change material. Energy Convers. Manag. 89, 833–842. https://doi.org/10.1016/j.enconman.2014.10.053

Wu, S., Zhu, D., Zhang, X., Huang, J., 2010. Preparation and melting/freezing characteristics of Cu/paraffin nanofluid as phase-change material (PCM). Energy and Fuels 24, 1894–1898. https://doi.org/10.1021/ef9013967

Abbreviations and Nomenclature

Table 1: Recommended symbols for materials properties

Quantity	Symbol	Unit
c_p	Specific heat	kJ kg^{-1} K^{-1}
$\vec{g}$	Gravitational acceleration	m sec^{-2}
H_t	Total enthalpy	kJ kg^{-1}
h_l	Enthalpy of phase change	kJ kg^{-1}
h_s	Specific sensible enthalpy	kJ kg^{-1}
k	Thermal conductivity	W/m^{-1} K^{-1}
L	Latent heat of PCM	kJ kg^{-1}
l	Length of the storage	m
m	Mass	kg
p	Pressure	Pa
r	Radial distance	m
R	Shell radius	m
T	Temperature	K
t	Time	s
$\vec{v}$	Velocity	m/s
z	Axial distance	m
Greek Symbols		
μ	Dynamic viscosity	Pa-s
ρ	Density	kg m^{-3}
θ	Angular distance	degrees
β	Melt fraction	-
β_t	Volumetric expansion coefficient	K^{-1}

Table 2: Recommended subscripts

Quantity	Symbol
Ambient	amb
Fluid (HTF)	f
Interface	itf
Inner	i
Melting	m
outer	o
Reference	ref
Storage	st